A&A 512, A31 (2010)
DOI: 10.1051/0004-6361/200913098

Astronomy & Astrophysics

Abundance anomaly of the ^{13}C species of CCH

N. Sakai[1], O. Saruwatari[1], T. Sakai[2], S. Takano[3], and S. Yamamoto[1]

[1] Department of Physics and Research Center for the Early Universe, The University of Tokyo, Bunkyo-ku, Tokyo 113-0033, Japan
e-mail: [nami;osamu]@taurus.phys.s.u-tokyo.ac.jp; yamamoto@phys.s.u-tokyo.ac.jp
[2] Institute of Astronomy, The University of Tokyo, Osawa, Mitaka, Tokyo, 181-8588, Japan
e-mail: sakai@ioa.s.u-tokyo.ac.jp
[3] Nobeyama Radio Observatory and Graduate University for Advanced Studies, Minamimaki, Minamisaku, Nagano 384-1305, Japan
e-mail: stakano@nro.nao.ac.jp

Received 10 August 2009 / Accepted 15 December 2009

ABSTRACT

Aims. We have observed the $N = 1-0$ lines of CCH and its ^{13}C isotopic species toward a cold dark cloud, TMC-1 and a star-forming region, L1527, to investigate the ^{13}C abundances and formation pathways of CCH.
Methods. The observations have been carried out with the IRAM 30 m telescope.
Results. We have successfully detected the lines of ^{13}CCH and C^{13}CH toward the both sources and found a significant intensity difference between the two ^{13}C isotopic species. The [C^{13}CH]/[^{13}CCH] abundance ratios are 1.6 ± 0.4 (3σ) and 1.6 ± 0.1 (3σ) for TMC-1 and L1527, respectively. The abundance difference between C^{13}CH and ^{13}CCH means that the two carbon atoms of CCH are not equivalent in the formation pathway. On the other hand, the [CCH]/[C^{13}CH] and [CCH]/[^{13}CCH] ratios are evaluated to be larger than 170 and 250 toward TMC-1, and to be larger than 80 and 135 toward L1527, respectively. Therefore, both of the ^{13}C species are significantly diluted in comparison with the interstellar ^{12}C/^{13}C ratio of 60. The dilution is discussed in terms of a behavior of ^{13}C in molecular clouds.

Key words. astrochemistry – ISM: molecules – ISM: abundances – ISM: individual objects: TMC-1 – ISM: individual objects: L1527

1. Introduction

The ^{13}C isotopic species of various abundant molecules have been detected in interstellar space. Their spectral lines are often employed to estimate the optical depths of the normal species lines, where the abundance ratio of the ^{13}C species relative to the normal species is assumed to be the same as the elemental abundance ratio of ^{12}C/^{13}C. In reality, the ratio can differ from molecule to molecule, and the ^{12}C/^{13}C ratios of molecules should contain rich information on formation processes of molecules, as in the case of deuterium fractionation (e.g. Watson 1974; Millar et al. 1989; Hirota et al. 2001; Caselli et al. 2002). However, few works have been reported on this aspect of the ^{12}C/^{13}C ratio. The only exception is the observation of the three ^{13}C species of HC_3N reported by Takano et al. (1998). They found that the abundance of HCC^{13}CN is significantly higher than the one for H^{13}CCCN and HC^{13}CCN in TMC-1, indicating that three carbon atoms are not equivalent in the formation pathways of HC_3N. This result supports the assumption that the neutral-neutral reaction between C_2H_2 and CN plays an important role in the production of HC_3N.

We recently reported on the abundance anomaly of the ^{13}C species of CCS in the young starless cores TMC-1 and L1521E (Sakai et al. 2007a). The abundance ratio of [CCS]/[C^{13}CS] in TMC-1 is determined to be 54 ± 5 (3σ), which is almost consistent with the interstellar [^{12}C]/[^{13}C] ratio of 60 (Lucas & Liszt 1998). On the other hand, the [CCS]/[^{13}CCS] ratio is found to be as high as 230 ± 130 (3σ), the [C^{13}CS]/[^{13}CCS] ratio being 4.2±2.3(3σ). This indicates that the two carbon atoms of CCS are nonequivalent in the main production process. For the nonequivalent processes, S + CCH, S$^+$ + CCH, and CH + CS can be considered. If the reactions including CCH are mainly responsible, the abundances of ^{13}CCH and C^{13}CH must be different as in the case of ^{13}CCS and C^{13}CS. However, Sakai et al. (2007a) could not confirm this because of the lack of observational data of ^{13}CCH and C^{13}CH, so that the reactions including CCH were not completely ruled out as the main production process. Since the CCS molecule is now widely used to study the chemical evolution of starless cores (e.g. Suzuki et al. 1992; Benson et al. 1998; Ohashi et al. 1999; Aikawa et al. 2003), a detailed understanding of its production pathways is very important both for astrophysics and astrochemistry. For this purpose, the observation of the ^{13}C species of CCH is essential. In addition, it is also useful for constraining the main production pathway of CCH itself, which is crucial for a quantitative test of chemical models of dense clouds.

However, observations of the ^{13}C species of CCH have been limited so far. Saleck et al. (1994) detected the C^{13}CH and ^{13}CCH ($N = 2-1$) lines toward the Orion A molecular cloud. They reported that the [C^{13}CH]/[^{13}CCH] ratio is 1.50 ± 0.15 by comparing the observed intensities, although they claimed that the result may suffer from calibration uncertainties. Turner (2001) detected the $N = 1-0$ lines of C^{13}CH and ^{13}CCH toward TMC-1. According to their data, the C^{13}CH line is more intense than the ^{13}CCH line by a factor of 2. In these previous reports, a possible difference between the abundances of the two ^{13}C isotopic species is not seriously considered, because the S/N ratio is not high enough to discuss the [C^{13}CH]/[^{13}CCH] ratio accurately. Therefore we have conducted sensitive observations of the C^{13}CH and ^{13}CCH lines toward a young starless core,

Table 1. Observed line parameters in TMC-1 and L1527.

Species	Transition	S^a	Frequency (GHz)	$T_{MB}{}^b$ (K)	Δv^b (km s^{-1})	$\int T_{MB} dv$ (3σ) (K km s^{-1})	rms^c (mK)	$V_{LSR}{}^b$ (km s^{-1})
			TMC-1					
CCH	$J = 3/2-1/2$ $F = 1-1$	0.17	87.284156(30)	1.538(55)	0.49(2)	0.795(13)	8.8	5.907(9)
$N = 1-0$	$J = 3/2-1/2$ $F = 2-1$	1.67	87.316925(4)	2.144(78)	0.59(3)	1.336(15)	8.7	5.869(11)
	$J = 3/2-1/2$ $F = 1-0$	0.83	87.328624(6)	1.571(59)	0.56(2)	0.924(15)	9.2	5.912(10)
	$J = 1/2-1/2$ $F = 1-1$	0.83	87.402004(5)	1.711(101)	0.55(4)	0.963(22)	13.4	5.853(16)
	$J = 1/2-1/2$ $F = 0-1$	0.33	87.407165(11)	1.549(110)	0.53(4)	0.860(21)	14.6	5.789(19)
	$J = 1/2-1/2$ $F = 1-0$	0.17	87.446512(23)	1.424(52)	0.52(2)	0.808(15)	9.5	5.914(9)
$C^{13}CH$	$J = 3/2-1/2$ $F_1 = 2-1$ $F = 5/2-3/2$	2.00	85.2293354(26)	0.059(5)	0.52(5)	0.032(5)	3.1	5.84(2)^d
$N = 1-0$	$J = 3/2-1/2$ $F_1 = 2-1$ $F = 3/2-1/2$	1.26	85.2328050(22)	0.035(6)	0.56(10)	0.020(5)	3.2	5.89(4)^d
	$J = 3/2-1/2$ $F_1 = 1-0$ $F = 3/2-1/2$	1.27	85.2569879(33)	0.041(5)	0.43(6)	0.019(4)	3.4	5.83(3)^d
	$J = 1/2-1/2$ $F_1 = 1-1$ $F = 1/2-3/2$	0.62	85.3039898(33)	0.021(4)^e	0.69(17)^e	0.014(6)^e	2.7	5.89(7)^{d,e}
	$J = 1/2-1/2$ $F_1 = 1-1$ $F = 3/2-3/2$	1.21	85.3074593(33)	0.034(4)	0.53(8)	0.020(5)	2.9	5.83(3)^d
^{13}CCH	$J = 3/2-1/2$ $F_1 = 2-1$ $F = 5/2-3/2$	2.00	84.119329(17)	0.037(4)	0.52(7)	0.020(4)	2.8	5.84(3)
$N = 1-0$	$J = 3/2-1/2$ $F_1 = 2-1$ $F = 3/2-1/2$	1.22	84.124143(20)	0.026(5)	0.46(10)	0.012(4)	2.8	5.80(4)
	$J = 1/2-1/2$ $F_1 = 0-1$ $F = 1/2-1/2$	0.46	84.183977(28)	0.026(5)^e	0.28(7)^e	0.007(3)^e	3.5	5.71(3)^e
			L1527					
CCH	$J = 3/2-1/2$ $F = 1-1$	0.17	87.284156(30)	1.932(19)	0.53(1)	1.112(20)	12.8	6.026(2)
$N = 1-0$	$J = 3/2-1/2$ $F = 2-1$	1.67	87.316925(4)	−−	−−	3.592(21)	13.3	−−
	$J = 3/2-1/2$ $F = 1-0$	0.83	87.328624(6)	−−	−−	2.447(23)	14.4	−−
	$J = 1/2-1/2$ $F = 1-1$	0.83	87.402004(5)	−−	−−	2.602(21)	13.3	−−
	$J = 1/2-1/2$ $F = 0-1$	0.33	87.407165(11)	2.775(25)	0.60(1)	1.801(24)	13.5	5.846(3)
	$J = 1/2-1/2$ $F = 1-0$	0.17	87.446512(23)	2.014(19)	0.52(1)	1.162(21)	13.3	6.011(2)
$C^{13}CH$	$J = 3/2-1/2$ $F_1 = 2-1$ $F = 5/2-3/2$	2.00	85.2293354(26)	0.163(10)	0.43(3)	0.078(6)	4.4	5.950(5)^f
$N = 1-0$	$J = 3/2-1/2$ $F_1 = 2-1$ $F = 3/2-1/2$	1.26	85.2328050(22)	0.104(10)	0.56(3)	0.060(7)	3.9	5.950(5)^f
	$J = 3/2-1/2$ $F_1 = 1-0$ $F = 1/2-1/2$	0.65	85.2477276(33)	0.058(7)	0.50(7)	0.028(6)	3.9	5.950(5)^f
	$J = 3/2-1/2$ $F_1 = 1-0$ $F = 3/2-1/2$	1.27	85.2569879(33)	0.098(8)	0.45(4)	0.047(6)	4.2	5.950(5)^f
	$J = 1/2-1/2$ $F_1 = 1-1$ $F = 1/2-3/2$	0.62	85.3039898(33)	0.046(5)	0.55(7)	0.026(4)	2.4	5.950(5)^f
	$J = 1/2-1/2$ $F_1 = 1-1$ $F = 3/2-3/2$	1.21	85.3074593(33)	0.110(7)	0.42(3)	0.050(3)	2.7	5.950(5)^f
	$J = 1/2-1/2$ $F_1 = 0-1$ $F = 1/2-1/2$	0.62	85.3140918(33)	0.051(5)	0.42(4)	0.024(4)	2.8	5.950(5)^f
^{13}CCH	$J = 3/2-1/2$ $F_1 = 2-1$ $F = 5/2-3/2$	2.00	84.119329(17)	0.093(5)	0.48(3)	0.047(2)	1.6	5.94(1)
$N = 1-0$	$J = 3/2-1/2$ $F_1 = 2-1$ $F = 3/2-1/2$	1.22	84.124143(20)	0.056(6)	0.53(7)	0.033(3)	1.6	5.95(3)
	$J = 3/2-1/2$ $F_1 = 1-0$ $F = 1/2-1/2$	0.66	84.151352(16)	0.030(5)	0.48(9)	0.015(2)	1.5	5.90(4)
	$J = 3/2-1/2$ $F_1 = 1-0$ $F = 3/2-1/2$	1.33	84.153305(15)	0.059(4)	0.51(4)	0.034(2)	1.4	5.89(2)
	$J = 1/2-1/2$ $F_1 = 0-1$ $F = 1/2-1/2$	0.46	84.183977(28)	0.024(3)	0.36(5)	0.011(2)	2.0	5.90(2)
	$J = 1/2-1/2$ $F_1 = 1-1$ $F = 1/2-3/2$	0.46	84.192487(30)	0.029(4)	0.50(8)	0.016(4)	2.8	5.90(3)
	$J = 1/2-1/2$ $F_1 = 1-1$ $F = 3/2-3/2$	1.22	84.206865(19)	0.067(3)	0.46(3)	0.033(2)	1.7	5.90(1)
	$J = 1/2-1/2$ $F_1 = 1-1$ $F = 1/2-1/2$	0.22	84.225376(20)	−−	−−	≤ 4.6	3.1	−−

Notes. The numbers in parentheses represent the errors in units of the last significant digits. [(a)] Intrinsic line strength. [(b)] Obtained by the Gaussian fit. [(c)] The rms noise at an emission free region averaged over the line width. For non detected lines, the line widths of 0.5 km s^{-1} are assumed. [(d)] Calculated on the basis of the rest frequencies of the $C^{13}CH$ lines obtained in this study (Table A.1). [(e)] Marginal detection. [(f)] See Sect. 3.1 and Appendix A.

TMC-1, and a star-forming core exibiting warm carbon-chain chemistry (Sakai et al. 2008), L1527, both of which are bright sources of CCH.

2. Observations

Observations of the $N = 1-0$ lines of CCH and its ^{13}C isotopic species were carried out with the IRAM 30 m telescope at Pico Veleta[1] in July 11–14, 2007. Transition frequencies and quantum numbers of the observed lines are listed in Table 1. The observed position was $(\alpha_{2000}, \delta_{2000}) = (04^h41^m42\overset{s}{.}88, 25°41'27\overset{''}{.}0)$ for the cyanopolyyne peak of TMC-1 (hereafter TMC-1) and $(\alpha_{2000}, \delta_{2000}) = (04^h39^m53\overset{s}{.}89, 26°03'11\overset{''}{.}0)$ for L1527. Two 3 mm SIS receivers (A100 and B100) were simultaneously used as frontends, whose system noise temperatures ranged from 75 K to 105 K for A100 and from 90 K to 130 K for B100. The beam size and the effective main-beam efficiency (B_{eff}/F_{eff}) of the telescope at 85 GHz are 29″ and 0.82, respectively (B_{eff} and F_{eff} are the main beam efficiency (0.78) and forward efficiency (0.95), respectively). The telescope pointing was checked every hour by observing nearby continuum sources and was maintained to be better than 4″. The backend was an autocorrelator, VESPA, which was divided into 12 parts to cover hyperfine components. We set the individual bandwidth and resolution to be 20 MHz and 20 kHz, respectively. The frequency resolution corresponds to the velocity resolution of 0.07 km s^{-1}.

The position-switching mode was employed for the observation of the normal species (CCH) toward L1527, where the off position was taken at $\Delta\alpha = 30'$, $\Delta\delta = 30'$. On the other hand, the other observations were made in the frequency-switching mode with a frequency offset of 2 MHz. Since the line width is much narrower (~0.5 km s^{-1}) than the period of the baseline ripple (~30 km s^{-1}), we can readily subtract the baseline for the 20 km s^{-1} span with the second or third order polynomial. For the observations of the ^{13}C isotopomers, we first used

[1] IRAM is supported by INSU/CNRS (France), MPG (Germany), and IGN (Spain).

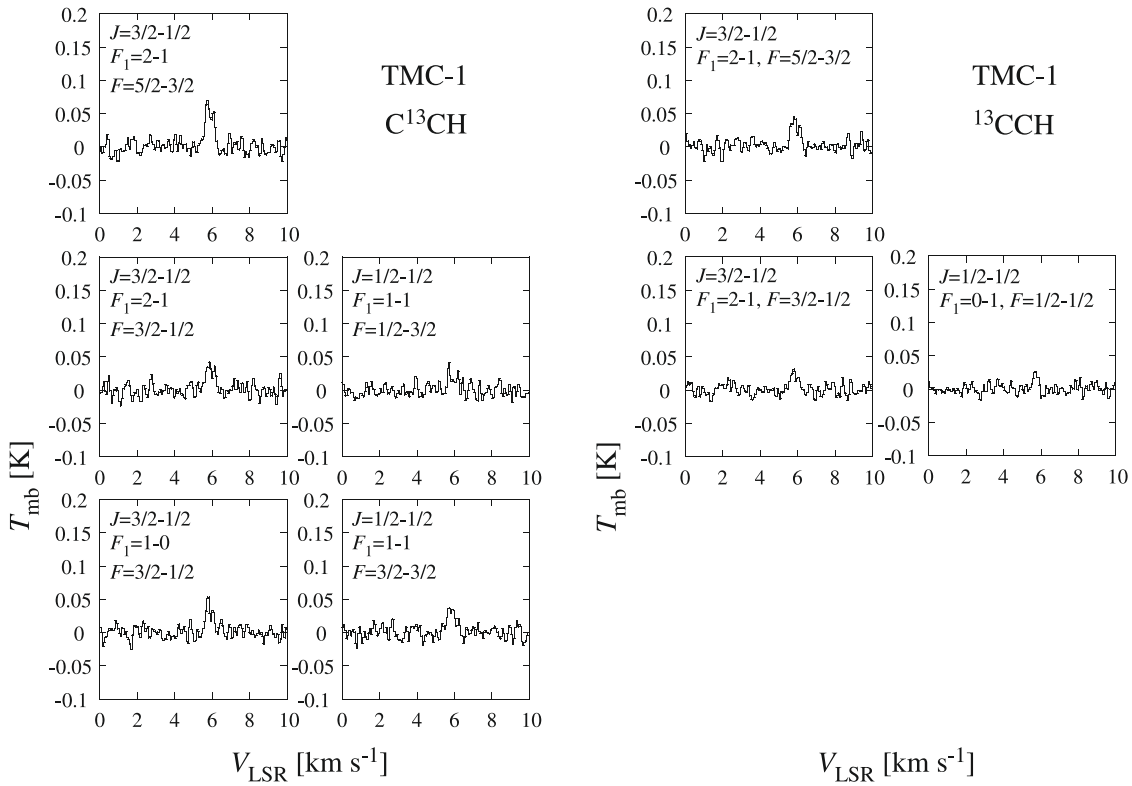

Fig. 1. Observed line profiles of the hyperfine components of the $N = 1-0$ transitions of C^{13}CH and ^{13}CCH in TMC-1.

the two 3 mm band receivers simultaneously, one for ^{13}CCH and the other for C^{13}CH, to minimize the pointing error and the telescope efficiency variation on the observed abundance ratio. We extended the observation of the ^{13}CCH lines toward L1527 with the two receivers to improve the S/N ratio after good quality spectra were obtained for the C^{13}CH lines in the simultaneous observation. In this case, the intensity scale of the ^{13}CCH lines was confirmed by comparing the intensities of the nearby strong lines (c-H^{13}CCCH $2_{12}-1_{01}$ and DC_3N $J = 10-9$) with those observed in the simultaneous observation of ^{13}CCH and C^{13}CH. Basic data reduction was carried out by the CLASS software.

3. Results

3.1. Detection of hyperfine components of C^{13}CH and ^{13}CCH

We successfully detected the hyperfine component lines of C^{13}CH and ^{13}CCH toward TMC-1 and L1527 (Table 1). We detected seven hyperfine components for each species in L1527, while in TMC-1 we detected five and three hyperfine components for C^{13}CH and ^{13}CCH, respectively. The line profiles in TMC-1 and L1527 are shown in Figs. 1 and 2, respectively. In the line assignment, we found that the $V_{\rm LSR}$ values of the ($J = 1/2-1/2, F_1 = 1-1, F = 3/2-3/2$) and ($J = 1/2-1/2, F_1 = 0-1, F = 1/2-1/2$) lines of C^{13}CH are shifted by 0.9 and 1.1 km s^{-1}, respectively, from the typical $V_{\rm LSR}$ value of L1527 (5.85–5.95 km s^{-1}) when we employed the rest frequencies listed in CDMS (Müller et al. 2005; McCarthy et al. 1995). A shift in the ($J = 1/2-1/2, F_1 = 1-1, F = 3/2-3/2$) line is also seen in TMC-1. These shifts seem to originate from uncertainties in the rest frequencies. In order to confirm this, we further checked the data of the same lines observed in the course of the line survey toward L1527 with the Nobeyama 45 m telescope[2] (e.g. Sakai et al. 2008). The $V_{\rm LSR}$ values of the above two lines were also found to be shifted by the same magnitudes as in the IRAM 30 m observation. Therefore it was confirmed that the rest frequencies are not accurate enough to analyze our C^{13}CH data, and we refined some molecular constants of C^{13}CH by fitting the line frequencies observed in L1527. Details of this procedure are described in Appendix A. The $V_{\rm LSR}$ value finally determined for L1527 is 5.950 ± 0.005 km s^{-1}, which is consistent with those for other molecules (e.g. Sakai et al. 2008). The frequencies of the hyperfine components are calculated from newly determined molecular constants and are used to derive the line parameters of C^{13}CH in TMC-1 (Table 1).

3.2. Abundance anomaly of the ^{13}C species of CCH

As shown in Fig. 1, the intensity of the strongest hyperfine component ($J = 3/2-1/2$ $F_1 = 2-1$ $F = 5/2-3/2$) of C^{13}CH in TMC-1 is found to be significantly stronger than that of ^{13}CCH. A fraction of the line intensity of the strongest hyperfine component relative to the total intensity of the all hyperfine components of the $N = 1-0$ transition is exactly the same for C^{13}CH and ^{13}CCH, although those of the other components vary between the two isotopic species. Since the excitation conditions can be regarded to be the same for C^{13}CH and ^{13}CCH, the intensity difference found for the strongest hyperfine components should directly reflect the difference in abundance of the two isotopic species. Note that the C^{13}CH and ^{13}CCH lines are optically thin, because the observed intensity ratios of the hyperfine components are close to the theoretical ones. Consequently we

[2] Nobeyama Radio Observatory is a branch of the National Astronomical Observatory of Japan, National Institutes of Natural Sciences, Japan.

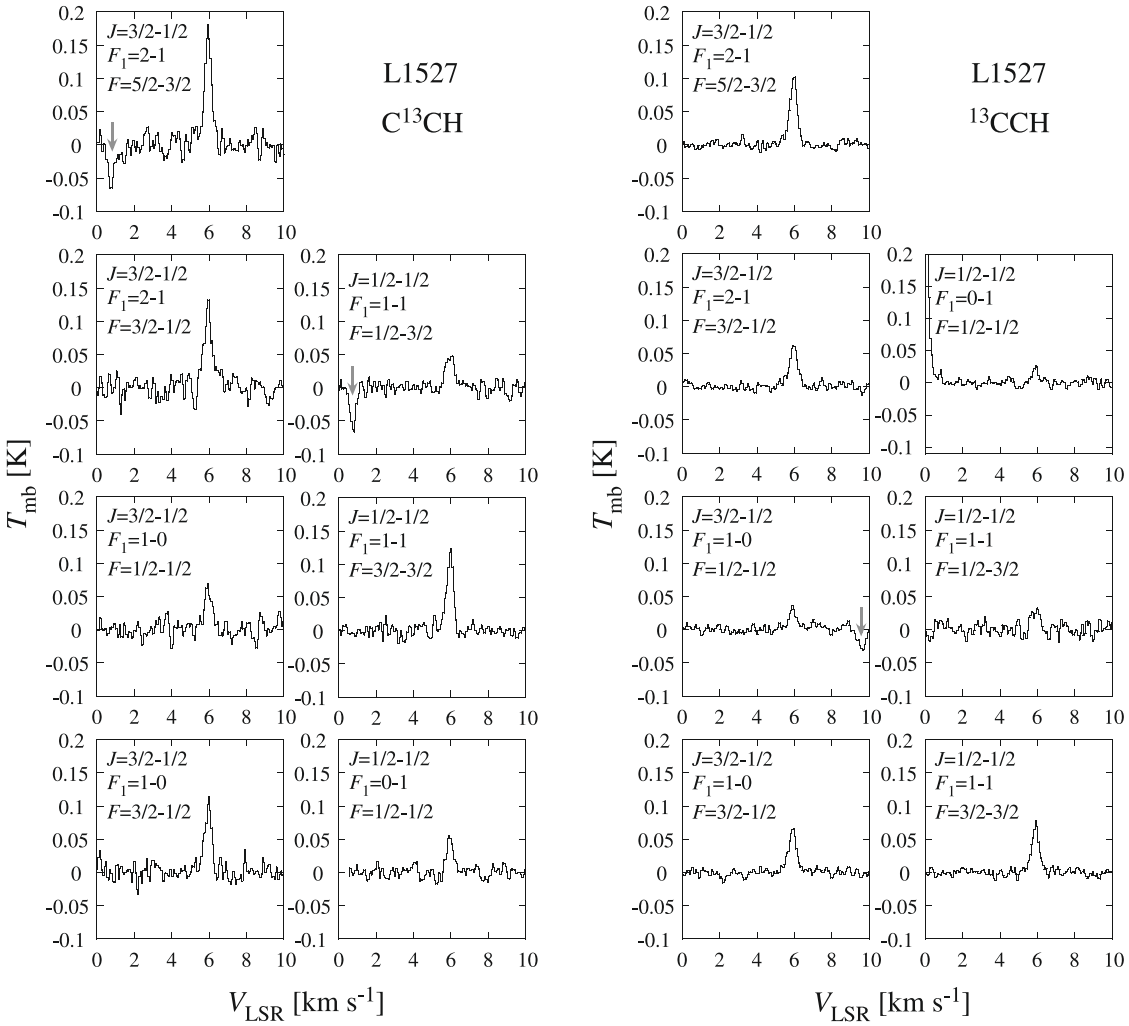

Fig. 2. Observed line profiles of the hyperfine components of the $N = 1-0$ transitions of $C^{13}CH$ and ^{13}CCH in L1527. Negative features indicated by arrows are frequency-switch artifacts of nearby lines. The line at V_{LSR} of about 0 km s^{-1} in the panel of the $J = 1/2-1/2$, $F_1 = 0-1$, $F = 1/2-1/2$ line for ^{13}CCH is the $2_{1,2}-1_{0,1}$ line of c-H^{13}CCCH.

can accurately estimate the abundance ratio of [$C^{13}CH$]/[^{13}CCH] from the observed integrated intensity ratio as long as the same excitation temperature is assumed for the both species. The [$C^{13}CH$]/[^{13}CCH] ratio is found to be 1.6 ± 0.4 (3σ) for TMC-1, where the error represents three times the standard deviation. A similar intensity difference is also observed for L1527, as shown in Fig. 2. In L1527, the [$C^{13}CH$]/[^{13}CCH] ratio is derived to be 1.6 ± 0.1 (3σ). Although we made a more detailed integration for ^{13}CCH than for $C^{13}CH$ toward L1527 to improve the S/N ratio, we confirmed that the line intensities of ^{13}CCH observed simultaneously with the $C^{13}CH$ lines are consistent with those finally obtained after the extended observation. Hence it is clearly established that the abundances of the two ^{13}C isotopic species are different, as in the case of HC_3N (Takano et al. 1998) and CCS (Sakai et al. 2007a). Since the H_2 densities of TMC-1 and L1527 are $\sim 3\times10^4$ (Sect. 3.3) and $>10^6$ cm^{-3} (Sakai et al. 2008), respectively, the result suggests that the [$C^{13}CH$]/[^{13}CCH] ratio does not strongly depend on the H_2 density.

As mentioned in the introduction, Saleck et al. (1994) reported the [$C^{13}CH$]/[^{13}CCH] ratio of 1.50 ± 0.15 in the Orion A molecular cloud, although they claimed that their result may suffer from calibration uncertainty. According to the $C^{13}CH$ and ^{13}CCH observations toward TMC-1 by Turner (2001), we can estimate the intensity ratio of the strongest hyperfine components to be two. Unfortunately, it is impossible to estimate the error because of a lack of information about uncertainties in the intensities, and hence we cannot judge whether this ratio is significant or not. In spite of the poor accuracy of the previous measurements, the trend that $C^{13}CH$ is more abundant than ^{13}CCH seems to be consistent with our result.

3.3. $C^{13}CH$ and ^{13}CCH abundances relative to CCH

In order to derive the abundance ratios of [CCH]/[$C^{13}CH$] and [CCH]/[^{13}CCH], the $N = 1-0$ lines of CCH were observed toward TMC-1 and L1527, as were those of $C^{13}CH$ and ^{13}CCH. In both sources, all hyperfine components except for the two weakest ones apparently look optically thick, judging from their line shapes and the intensity ratios among the hyperfine components (Table 1, Fig. 3). In particular, self-absorption dips are obvious in a few stronger components observed toward L1527, so even the weakest hyperfine components may not be optically thin. We then derived the lower limit of the column density of CCH from the integrated intensities of the weakest hyperfine components ($J = 1/2-1/2$, $F = 1-0$ and $J = 3/2-1/2$, $F = 1-1$). On the other hand, we used all the available hyperfine component data to derive the column densities of $C^{13}CH$ and ^{13}CCH.

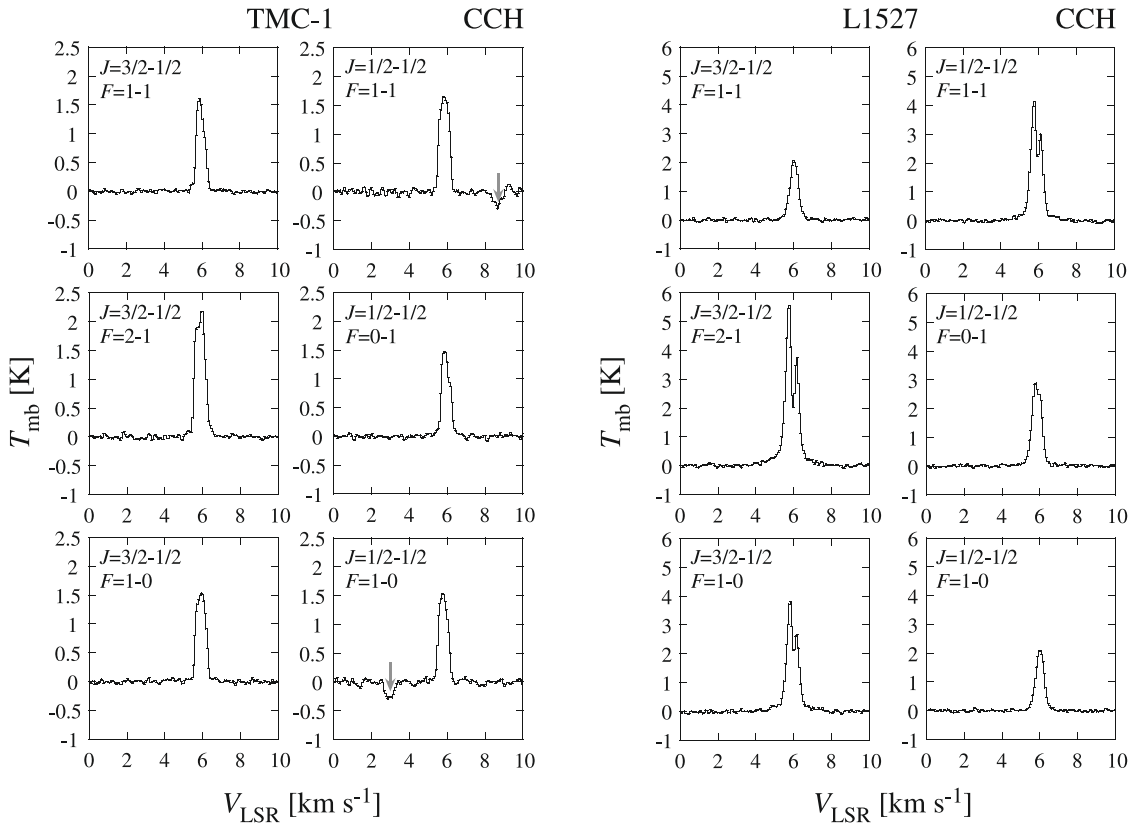

Fig. 3. Observed line profiles of the hyperfine components of the $N = 1-0$ transitions of CCH in TMC-1 and L1527. Negative features indicated by arrows are frequency switch artifacts of nearby lines.

In derivation of the column densities of CCH and its ^{13}C species, we employed the one-zone large velocity gradient (LVG) model for excitation calculations (Goldreich & Kwan 1974). As mentioned above, the optical depths of the CCH lines are very different from those of the ^{13}C species, so that their excitation temperatures can be different. In this case, the LTE approximation with the common excitation temperature may introduce a systematic error in the derived abundance ratios. This renders a statistical equilibrium calculation like the LVG model indispensable. Since the collisional cross sections are not reported for CCH, we adopted the corresponding values of a similar-sized molecule, HCN (Green & Thaddeus 1974). We fully considered the fine- and hyperfine-structure levels up to $N = 10$ (42 and 82 for CCH and its ^{13}C species, respectively), and evaluated the collisional cross sections between two hyperfine levels by the method described in Appendix B. We employed the photon escape probability for a spherical cloud. The dipole moment is assumed to be 0.8 D for all the three isotopic species (CCH, ^{13}CCH, C^{13}CH). The velocity width of 0.6 km s^{-1} is employed for the velocity gradient for the both sources.

The column density of CCH toward TMC-1 is determined to be $(6.5 \pm 2.7) \times 10^{14}$ cm^{-2} from the intensities of the two weakest hyperfine components by a least-squares method, where the H_2 density and the gas kinetic temperature are assumed to be 3×10^4 cm^{-3} and 10 K, respectively. The optical depth of the weakest component, $J = 1/2-1/2$ $F = 1-0$, is calculated to be 0.4. The column densities of C^{13}CH and ^{13}CCH in TMC-1 are also evaluated by a least-squares method from the observed intensities of all the hyperfine components to be $(3.9 \pm 0.4) \times 10^{12}$ cm^{-2} and $(2.6 \pm 0.4) \times 10^{12}$ cm^{-2}, respectively. Here the errors represent three times the standard deviation. The column density of CCH is regarded as a lower limit, considering the possible self absorption effect due to the foreground gas, as mentioned above. Then, we can set the lower limits to the abundance ratios of [CCH]/[C^{13}CH] and [CCH]/[^{13}CCH] to be 170 and 250, respectively, from the obtained column densities. On the other hand, the [C^{13}CH]/[^{13}CCH] ratio is derived to be 1.5 ± 0.3, which is consistent with the ratio derived from the integrated intensities in Sect. 3.2.

The dependence of these values on the assumed H_2 density is shown in Fig. 4a. In the density range between 10^4 cm^{-3} and 10^5 cm^{-3}, which is appropriate for TMC-1 (Hirahara et al. 1992; Hirota et al. 1998), the abundance ratios [CCH]/[C^{13}CH] and [CCH]/[^{13}CCH] increase as a function of the density, whereas the [C^{13}CH]/[^{13}CCH] ratio almost remains constant. From Fig. 4a, the abundance ratios of [CCH]/[C^{13}CH] and [CCH]/[^{13}CCH] are higher than 130 and 190, respectively, even if the density is as low as 10^4 cm^{-3}. These values are much higher than the interstellar [^{12}C]/[^{13}C] ratio of 60 (Lucus & Liszt 1998). This means that both the ^{13}C species of CCH are heavily diluted in TMC-1, as in the case of ^{13}CCS (230 ± 130) (Sakai et al. 2007a). To confirm this, we derived the abundance ratios of [CCH]/[C^{13}CH] and [CCH]/[^{13}CCH] under the assumption of LTE conditions with the excitation temperature of 6.7 K, which is reported for C_6H in TMC-1 (Sakai et al. 2007b). The [CCH]/[C^{13}CH] and [CCH]/[^{13}CCH] ratios are derived to be 160^{+50}_{-20} and 250^{+80}_{-50}, respectively, from the obtained column densities, where the column density of CCH is evaluated from the intensities of the two weakest hyperfine components. These are almost consistent with those derived from the LVG model analysis.

The column densities of CCH, C^{13}CH and ^{13}CCH are also determined for L1527 by the use of the LVG model. For L1527, the H_2 density and the gas kinetic temperature are assumed to be

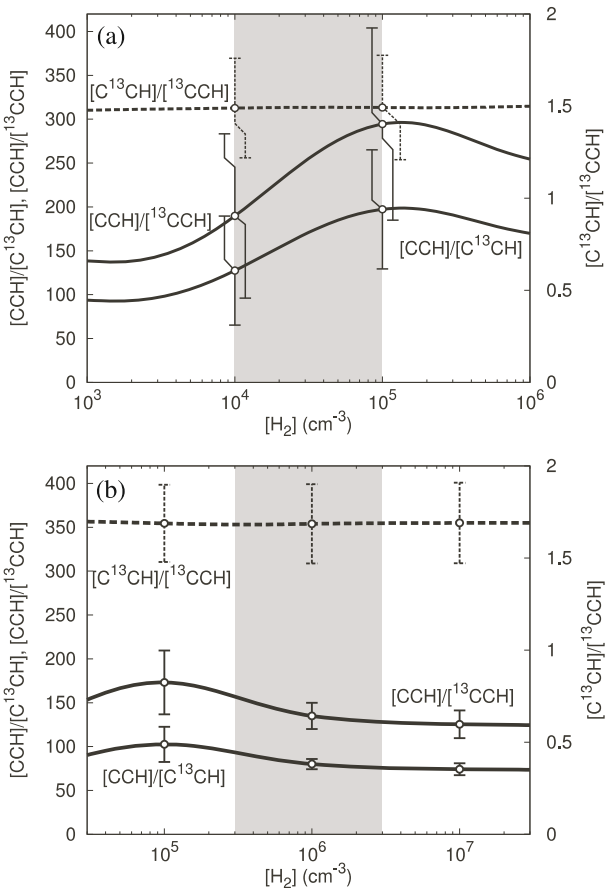

Fig. 4. Results of the LVG model calculations for TMC-1 **a**) and L1527 **b**). The solid lines represent the [CCH]/[C^{13}CH] and [CCH]/[^{13}CCH] ratios, whereas the dashed line represents the [C^{13}CH]/[^{13}CCH] ratio. Shaded areas are appropriate density ranges for the sources. The error bars denote three times the standard deviations.

10^6 cm^{-3} and 15 K, respectively (Sakai et al. 2008). The column density of CCH is determined to be $(9.8 \pm 0.2) \times 10^{14}$ cm^{-2} from the two weakest hyperfine components, whereas those of C^{13}CH and ^{13}CCH are $(1.2 \pm 0.1) \times 10^{13}$ and $(7.3 \pm 0.8) \times 10^{12}$ cm^{-2}, respectively. The optical depth of the weakest component of CCH, $J = 1/2-1/2$ $F = 1-0$, is calculated to be 0.2. The [CCH]/[C^{13}CH] and [CCH]/[^{13}CCH] ratios are thus derived to be 80 and 135, respectively. Since the CCH lines may suffer from the self absorption effect due to the foreground gas, the ratios should be regarded as the lower limits. On the other hand, the [C^{13}CH]/[^{13}CCH] ratio is derived to be 1.7 ± 0.2, which is consistent with the ratio derived from the integrated intensities. The density dependence of the ratios is shown in Fig. 4b. For the density range from 3×10^5 cm^{-3} to 3×10^6 cm^{-3}, the ratios slightly decrease as the density increases. Even for the density of 3×10^6 cm^{-3}, the [CCH]/[C^{13}CH] and [CCH]/[^{13}CCH] ratios are 75 and 130, respectively. Thus, it is very likely that the ratios in L1527 are larger than the interstellar [^{12}C]/[^{13}C] ratio of 60, as in the case of TMC-1. For confirmation, we also calculated the [CCH]/[C^{13}CH] and [CCH]/[^{13}CCH] ratios to be 88^{+8}_{-9} and 140 ± 10 under the assumption of LTE conditions. Here we assume the excitation temperature of 12.3 K reported for C_4H_2 (Sakai et al. 2008). These ratios are consistent with those derived by the LVG analysis.

Table 3 summarizes the [CCH]/[C^{13}CH] and [CCH]/[^{13}CCH] ratios obtained with the LVG analyses. As for the [C^{13}CH]/[^{13}CCH] ratio, we adopt the values derived from the integrated intensity ratios of the strongest hyperfine components (Sect. 3.2).

Table 2. The column densities of CCH and its ^{13}C isotopic species.

Model	Species	TMC-1 [cm^{-2}]	L1527 [cm^{-2}]
LVG[a]	CCH	$(6.5 \pm 2.7) \times 10^{14}$	$(9.8 \pm 0.2) \times 10^{14}$
	C^{13}CH	$(3.9 \pm 0.4) \times 10^{12}$	$(1.2 \pm 0.1) \times 10^{13}$
	^{13}CCH	$(2.6 \pm 0.4) \times 10^{12}$	$(7.3 \pm 0.8) \times 10^{12}$
LTE[b]	CCH	$(5.4 \pm 0.1) \times 10^{14}$	$(8.1^{+0.1}_{-0.2}) \times 10^{14}$
	C^{13}CH	$(3.4^{+0.5}_{-0.7}) \times 10^{12}$	$(9.3 \pm 0.7) \times 10^{12}$
	^{13}CCH	$(2.1 \pm 0.5) \times 10^{12}$	$(5.7 \pm 0.3) \times 10^{12}$

Notes. The errors quoted represent three times the standard deviation. [(a)] The H_2 densities and the gas kinetic temperatures are assumed to be 3×10^4 and 10 K, 1×10^6 cm^{-3} and 15 K, for TMC-1 and L1527, respectively. [(b)] The excitation temperatures are assumed to be 6.7 K and 12.3 K for TMC-1 and L1527, respectively.

Table 3. The abundance ratio of CCH and its ^{13}C isotopic species.

Ratio	TMC-1	L1527
[CCH]/[C^{13}CH][a]	≥170	≥80
[CCH]/[^{13}CCH][b]	≥250	≥135
[C^{13}CH]/[^{13}CCH][b]	1.6(4)	1.6(1)

Notes. The numbers in parentheses represent the three sigma errors in units of the last significant digits. [(a)] Derived from the LVG model. [X] represents the abundance of X, and the [X]/[Y] ratio can be obtained from the column densities of X and Y, assuming that both molecules exist in the same region. [(b)] Derived from the integrated intensity ratio of the strongest hyperfine components of C^{13}CH and ^{13}CCH.

4. Discussion

4.1. Abundance difference between C^{13}CH and ^{13}CCH

We have found that the abundances of C^{13}CH and ^{13}CCH are different from each other both in TMC-1 and L1527. Here we discuss two possible mechanisms; one is related to the main production pathway of CCH, and the other is the exchange of the ^{13}C position after formation of CCH.

As for the production mechanisms of CCH, the following major pathways have been considered. The first scheme is based on ion-molecule reactions, where CCH is mainly produced by electron recombination reactions of the precursor ions $C_2H_2^+$ and $C_2H_3^+$ as

$$C_2H_2^+ + e \rightarrow C_2H + H, \quad (1a)$$

and

$$C_2H_3^+ + e \rightarrow C_2H + H_2. \quad (1b)$$

The second scheme is a neutral-neutral reaction (e.g. Turner et al. 2000)

$$CH_2 + C \rightarrow C_2H + H. \quad (2)$$

However, their relative importance has not been established observationally. In the ion-molecule reaction scheme, the two carbon atoms are identical. Note that $C_2H_3^+$ has a non classical structure with the two identical carbon atoms (Crofton et al. 1989). In contrast, two carbon atoms are not equivalent for the neutral-neutral reaction (2). Therefore the difference in the abundances

of C^{13}CH and ^{13}CCH would reflect the significant contribution of reaction (2).

Yet there are two possibilities which would change the [C^{13}CH]/[^{13}CCH] ratio after the formation of CCH. One is the proton transfer reaction from protonated ions like HCO$^+$ and H_3^+. With this reaction followed by the dissociative electron recombination reaction of H^{13}CCH$^+$, the abundances of C^{13}CH and ^{13}CCH are equalized, because the branching ratio to C^{13}CH and ^{13}CCH of the electron recombination reaction should be the same. The other is the neutral-neutral reaction with the atomic hydrogen

$$^{13}\mathrm{CCH} + \mathrm{H} \rightarrow \mathrm{C}^{13}\mathrm{CH} + \mathrm{H} + 8.1\ \mathrm{K}. \quad (3)$$

Since C^{13}CH is more stable than ^{13}CCH by 8.1 K (Tarroni, private communication; Tarroni & Carter 2003), this reaction would enhance the abundance of C^{13}CH relative to that of ^{13}CCH. However, it is not clear whether this reaction actually happens in a cold cloud like TMC-1 or not. According to Rodgers & Millar (1996) and Schilke et al. (1992), a related reaction,

$$\mathrm{CCH} + \mathrm{D} \rightarrow \mathrm{CCD} + \mathrm{H}, \quad (4)$$

has an activation barrier of 250 K. If so, reaction (3) should also have an activation barrier of the same magnitude. In this case, reaction (3) does not contribute to the abundance difference between C^{13}CH and ^{13}CCH. Even if it has no activation barrier, a simplified chemical model considering reaction (3) does not reproduce the observed [C^{13}CH]/[^{13}CCH] ratio for L1527, as described in Appendix C. This is because reaction (3) is slower than the destruction reaction of CCH with the oxygen atom. Therefore, reaction (3) is not the main process to produce the abundance difference between C^{13}CH and ^{13}CCH, and the abundance differences reflect the contribution of reaction (2), as described above.

4.2. Implications to production pathways of CCS

As described in the introduction, we recently discovered the abundance difference between C^{13}CS and ^{13}CCS in TMC-1 and L1521E (Sakai et al. 2007a). The [C^{13}CS]/[^{13}CCS] ratio is $4.2 \pm 2.3 (3\sigma)$ in TMC-1, indicating that the two carbon atoms in CCS are not equivalent in the main production pathways. Thus the $S^+ + C_2H_2$ reaction, which has long been thought to be important, is ruled out as the main process. As for the other routes, reactions involving CCH have been thought to be

$$\mathrm{S}^+ + \mathrm{C_2H} \rightarrow \mathrm{C_2S}^+ + \mathrm{H} \quad (5a)$$

$$\mathrm{C_2S}^+ + \mathrm{H_2} \rightarrow \mathrm{HCCS}^+ + \mathrm{H} \quad (5b)$$

$$\mathrm{HCCS}^+ + \mathrm{e} \rightarrow \mathrm{CCS} + \mathrm{H} \quad (5c)$$

and

$$\mathrm{C_2H} + \mathrm{S} \rightarrow \mathrm{CCS} + \mathrm{H}. \quad (6)$$

Sakai et al. (2007a) considered that the difference in the abundances of C^{13}CH and ^{13}CCH might be transferred to CCS, but they could not discuss this further because of a lack of accurate observational data of the [C^{13}CH]/[^{13}CCH] ratio. Now the abundances of C^{13}CH and ^{13}CCH are determined accurately and we can examine the contribution of reactions (5) and (6) for production of CCS. In reaction (6), the sulfur atom will attack the end carbon atom of CCH to form the CCS structure, because the unpaired electron is on the end carbon atom (Yamada et al. 2002). The reaction (5a) is expected to occur in a similar way. Therefore the carbon atom next to the sulfur atom in CCS comes from the end carbon atom of CCH, as far as no migration of the carbon atoms does occur. This means that ^{13}CCS and C^{13}CS are produced from C^{13}CH and ^{13}CCH, respectively. If the reactions including CCH are mainly responsible for the CCS production, the [C^{13}CH]/[^{13}CCH] ratio should be lower than 1/4.2. However, the [C^{13}CH]/[^{13}CCH] ratio in TMC-1 is much different (1.6 ± 0.4). Furthermore, C^{13}CH and ^{13}CCH are significantly diluted compared with the interstellar ^{12}C/^{13}C ratio of 60, and hence it seems difficult to realize the [CCS]/[C^{13}CS] ratio of 54 by the production pathways involving CCH. Therefore, the production of CCS through CCH would be ruled out, and the main pathway seems to be the CS + CH reaction, as proposed by Sakai et al. (2007a).

Here it should be noted that the following exchange reaction could enhance the abundance of C^{13}CS relative to that of ^{13}CCS after the formation of CCS

$$^{13}\mathrm{CCS} + \mathrm{S} \rightarrow \mathrm{C}^{13}\mathrm{CS} + \mathrm{S} + 15\ \mathrm{K}. \quad (7)$$

This reaction is exothermic due to the difference in the zero-point vibrational energy (Y. Osamura, private communication). However, it is not obvious whether this reaction occurs in a cold cloud. This exchange reaction competes with the reaction producing ^{13}CS and CS. Furthermore, reaction (7) also competes with the destruction reactions of CCS by C$^+$, He$^+$, and H$^+$, and hence it would be difficult to realize the large abundance difference observed for C^{13}CS and ^{13}CCS. If CCS is produced from CCH and the exchange reaction (7) works, all ^{13}C atoms in CCH should go to C^{13}CS. Even in this extreme case, the [CCS]/[C^{13}CS] ratio is expected to be about 100, which is twice as large as the observed ratio (54). Although the contributions of reaction (7) to the [C^{13}CS]/[^{13}CCS] ratio is considered to be small for the above reasons, reaction (7) should be carefully studied by quantum chemical calculations.

4.3. ^{13}C dilution in CCH

The present results clearly show the dilution of ^{13}C in CCH. This is particularly significant in TMC-1. Here we discuss the mechanism of the dilution.

In dense molecular clouds where the interstellar UV radiation is well shielded, the main reservoir of ^{13}C is ^{13}CO, which is the most abundant carbon-bearing molecule. Note that the isotope selective photodissociation of CO is ineffective in this condition. The ^{13}C$^+$ ion is formed from ^{13}CO by the reaction with He$^+$, as ^{12}C$^+$ is formed from ^{12}CO. The ^{13}C$^+$ ion thus formed immediately reacts with ^{12}CO through the exothermic reaction as

$$^{13}\mathrm{C}^+ + \mathrm{CO} \rightarrow\ ^{13}\mathrm{CO} + \mathrm{C}^+ + 35\ \mathrm{K}. \quad (8)$$

Since the backward reaction of (8) is slow for a cold cloud, the [^{12}C$^+$]/[^{13}C$^+$] ratio becomes high due to a loss of ^{13}C$^+$ through reaction (8). This means that ^{13}C is diluted in C$^+$. Hence various organic molecules including CCH produced from C$^+$ in the gas phase would show the dilution of the ^{13}C species (Fig. 5). On the other hand, the [^{12}CO]/[^{13}CO] ratio almost remains at the ^{12}C/^{13}C interstellar ratio of 60. The HCO$^+$ and CO_2 molecules, which are produced from CO, would also have the similar ratios. This was pointed out many years ago by Langer et al. (1984). Its observational confirmation has been very difficult so far because of observational difficulties such as weak intensities of the ^{13}C species lines and heavy saturation of the normal species lines. The present result for CCH is a clear evidence supporting their theoretical prediction.

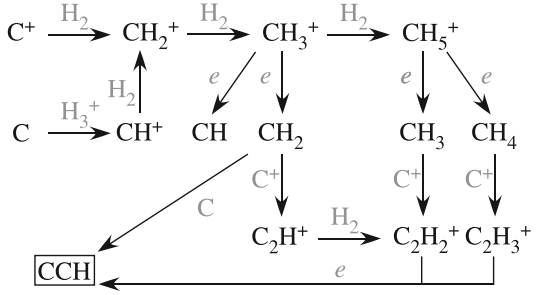

Fig. 5. Formation pathways of CCH.

So far the $^{12}C/^{13}C$ ratios have been reported for a few carbon-chain molecules in TMC-1. Takano et al. (1998) reported the $[HC_3N]/[H^{13}CCCN]$, $[HC_3N]/[HC^{13}CCN]$, and $[HC_3N]/[HCC^{13}CN]$ ratio to be 79 ± 11, 75 ± 10, and 55 ± 7 (1σ), respectively. Takano et al. (1990) derived the $^{12}C/^{13}C$ ratios for the five ^{13}C species of HC_5N to be 79–103. Recently, Langston & Turner (2007) reported the average $^{12}C/^{13}C$ ratios of HC_7N to be 87^{+35}_{-19} (1σ) respectively. Sakai et al. (2007a) also found the [CCS]/[$C^{13}CS$] and [CCS]/[^{13}CCS] ratios to be 54 ± 5 and 230 ± 130 (3σ), respectively. These results would suggest the dilution of ^{13}C in comparison with the interstellar $^{12}C/^{13}C$ ratio of 60 except for $[HC_3N]/[HCC^{13}CN]$ and [CCS]/[$C^{13}CS$]. However, the dilution has not been discussed seriously, although Sakai et al. (2007a) considered an effect of the isotope selective photodissociation for the ^{13}CCS case. Our result for CCH along with these early results now establishes that the ^{13}C species of the carbon-chain molecules are heavily diluted in TMC-1. Furthermore, these results mean that it is not possible to determine the elemental $^{12}C/^{13}C$ ratio from carbon-chain molecules.

A recent chemical model calculation by Woods & Willacy (2009) predicts the dilution of the ^{13}C species for various organic molecules except for CO and CO_2. For instance, the $^{12}C/^{13}C$ ratio for CCH is 118, although they do not treat two ^{13}C isotopic species separately. Unfortunately they do not provide the results using the best physical parameters for TMC-1 and L1527, because their purposes are to derive the initial condition for a simulation of the ^{13}C species in protoplanetary disks. Nevertheless, our results are roughly consistent with theirs.

As described in Sect. 3.2, $C^{13}CH$ is more abundant than ^{13}CCH. If the reaction (2) is responsible for the difference, the $^{12}C/^{13}C$ ratio in C should be higher than that in CH_2. Although such a difference would be possible in general, quantitative interpretation of this result requires a detailed chemical model treating two ^{13}C species separately, and is left for future studies.

As shown in Table 3, the [CCH]/[^{13}CCH] and [CCH]/[$C^{13}CH$] ratios seem to be higher for TMC-1 than for L1527, although the derived ratios are all lower limits. The difference between the two sources, if it exists, is very important. It may reflect the chemical evolutionary effect or can be related to the nature of each source. Langer & Graedel (1989) modeled the time evolution of the $^{12}C/^{13}C$ ratios of various species and found that the ratios increase as a function of time toward the steady-state. This is in contrast to the observation, since L1527 should be more evolved than TMC-1. Still, a depletion of CO onto dust grains is not incorporated in the model by Langer and Graedel, which may affect the $^{12}C/^{13}C$ ratio in the later stage. Alternatively, it is known that L1527 is a unique star-forming region showing warm carbon-chain chemistry (WCCC), where various carbon-chain molecules are abundant around the protostar (Sakai et al. 2008). A contribution of WCCC to the $^{12}C/^{13}C$ ratios is still unknown. Furthermore, the effect of the isotope selective photodissociation (e.g. Sonnentrucker et al. 2007) might have to be considered when we discuss the ^{13}C abundances during cloud formation and evolution. Therefore, detailed gas-grain chemical models considering gravitational contraction would be necessary toward a full understanding of a behavior of ^{13}C species in molecular clouds.

4.4. Summary

The $N = 1–0$ spectral lines of ^{13}CCH and $C^{13}CH$ have been detected toward a cold dark cloud, TMC-1, and a low-mass star forming region, L1527. The principal results are as follows.

1. The abundance ratio of [$C^{13}CH$]/[^{13}CCH] is determined to be 1.6 ± 0.4 (3σ) and 1.6 ± 0.1 (3σ) for TMC-1 and L1527, respectively, from the integrated intensity ratios of the strongest hyperfine components, where the errors quoted represent three times the standard deviation. It is now established that the abundances of $C^{13}CH$ and ^{13}CCH are significantly different.
2. The difference between the $C^{13}CH$ and ^{13}CCH abundances most likely originates from production pathways of CCH in TMC-1 and L1527. In this case, two carbon atoms must be nonequivalent in the production mechanism. Hence, the electron recombination reactions of $C_2H_2^+$ and $C_2H_3^+$ cannot explain the difference because of the equivalence of two carbon atoms in these ions. The neutral-neutral reaction, C + CH_2, would significantly contribute to the formation of CCH.
3. The [CCH]/[$C^{13}CH$] and [CCH]/[^{13}CCH] ratios are found to be larger than 170 and 250, respectively, for TMC-1, and to be larger than 80 and 135, respectively for L1527. These ratios are larger than the interstellar $^{12}C/^{13}C$ ratio of 60 for both of the sources, the ^{13}C isotope being diluted in CCH.
4. A similar trend of the ^{13}C dilution can be seen in the literature for some carbon-chain molecules like HC_3N, HC_5N, HC_7N, and CCS. However, it has not been seriously considered in previous observational studies. The dilution is now established observationally, which is consistent with the theoretical predictions by Langer et al. (1984) and Woods & Willacy (2009). Furthermore, the present results suggest that it is impossible to determine the $^{12}C/^{13}C$ elemental ratio from the carbon-chain molecules because of the positional differences and the heavy dilution.
5. The abundance difference between $C^{13}CH$ and ^{13}CCH and a source-to-source variation of the ^{13}C dilution are important problems left for future observational and theoretical studies.

Acknowledgements. The authors wish to thank Riccardo Tarroni for providing the zero-point vibrational energies of $C^{13}CH$ and ^{13}CCH, and Yoshihiro Osamura and Evelyne Roueff for valuable discussions. The authors are grateful to staff of the IRAM 30 M telescope for excellent support. This study is supported by Grant-in-Aids from the Ministry of Education, Culture, Sports, Science, and Technologies (21224002, 21740132, 15071201, and 19-6825).

Appendix A: Frequency of $C^{13}CH$

The frequencies of the fine and hyperfine component lines of $C^{13}CH$ ($N = 1–0$) observed in L1527 are used to refine the fine and hyperfine structure constants. In the analysis, the Hund's case $b_{\beta J}$ basis set (see Appendix B) is used to construct the Hamiltonian matrix, where all the off-diagonal matrix elements are included. The energy levels are obtained by direct diagonalization of the matrix. The fine and hyperfine structure constants

Table A.1. Observed and calculated frequencies of C^{13}CH (N = 1–0).

Transitions	ν_{obs}[a] [MHz]	$\Delta\nu$[b] [MHz]
J = 3/2–1/2 F_1 = 2–1 F = 5/2–3/2	85229.3354	–0.0021
J = 3/2–1/2 F_1 = 2–1 F = 3/2–1/2	85232.8050	0.0025
J = 3/2–1/2 F_1 = 1–0 F = 1/2–1/2	85247.7276	–0.0003
J = 3/2–1/2 F_1 = 1–0 F = 3/2–1/2	85256.9879	–0.0002
J = 1/2–1/2 F_1 = 1–1 F = 1/2–3/2	85303.9898	0.0004
J = 1/2–1/2 F_1 = 1–1 F = 3/2–3/2	85307.4593	–0.0001
J = 1/2–1/2 F_1 = 0–1 F = 1/2–1/2	85314.0918	–0.0003

Notes. [(a)] Observed rest frequencies are calculated assuming V_{LSR} of 5.950 km s^{-1}. [(b)] $\Delta\nu = \nu_{obs} - \nu_{calc.}$

Table A.2. Molecular constants for C^{13}CH.

Constant	
B	42631.383 (fixed)
D	0.10157 (fixed)
γ	–60.960(3)
b(^{13}C)	140.77(7)
c(^{13}C)	64.09(3)
b(H)	40.48(3)
c(H)	12.182(12)
V_{LSR}	5.950(5)

Notes. Units are in MHz except for V_{LSR} which is in km s^{-1}, B and D are taken from McCarthy et al. (1995). The numbers in parentheses represent one standard deviation in units of the last significant digits. Note that the rotational constants of CCH and ^{13}CCH are 43674.52894 MHz (Müller et al. 2000) and 42077.462 MHz (McCarthy et al. 1995), respectively.

are determined by a least-squares analysis. The spin-rotation interaction constant γ, the Fermi contact term (b) and the dipolar interaction term (c) for the ^{13}C and H nuculei are determined. Since the rotational and centrifugal distortion constants are accurately reported, they are fixed in the analysis. Instead, we optimize the correction for V_{LSR} as a parameter in the analyses. Seven lines listed in Table A.1 are successfully fitted within the observational errors. The standard deviation of the fit is 3.3 kHz. The result of the fit is shown in Table A.1, whereas the determined parameters are listed in Table A.2. The obtained constants are similar to those reported previously (McCarthy et al. 1995), and are used to calculate the rest frequencies of the hyperfine components (Table 1).

Appendix B: Collisional cross section of CCH

CCH is a free radical with an unpaired electron and has a $^2\Sigma^+$ ground electronic state. Because of the presence of both an electron spin and a nuclear spin of the hydrogen nucleus, the rotational energy levels are split into the fine and hyperfine structure levels. For the ^{13}C species of CCH, the levels are also split by the nuclear spin of ^{13}C. Here we briefly describe the calculations of the collisional transition rates among these energy levels, which are necessary for the LVG model calculation.

The following coupling scheme of the angular momenta (Hund's case b$_{\beta J}$) is employed for CCH in the present calculation

$$\boldsymbol{J} = \boldsymbol{N} + \boldsymbol{S}$$

and

$$\boldsymbol{F} = \boldsymbol{J} + \boldsymbol{I}(\mathrm{H}),$$

where $\boldsymbol{N}$, $\boldsymbol{S}$, and $\boldsymbol{I}$(H) denote the angular momenta of the end-over-end rotation, the electron spin (S = 1/2), and the nuclear spin of the hydrogen nuclei ($I(H)$ = 1/2). In the case of the ^{13}C species, the coupling scheme is as follows

$$\boldsymbol{F}_1 = \boldsymbol{J} + \boldsymbol{I}(^{13}\mathrm{C}),$$

and

$$\boldsymbol{F} = \boldsymbol{F}_1 + \boldsymbol{I}(\mathrm{H}),$$

where $\boldsymbol{I}$(^{13}C) is the angular momentum of the nuclear spin of the ^{13}C nucleus ($I(^{13}C)$ = 1/2). Then the energy levels can be labeled by the quantum numbers (N, J, F) for CCH and (N, J, F_1, F) for its ^{13}C species.

The collisional cross sections between two energy levels are calculated under the assumption of the infinite order-sudden (IOS) approximation (Alexander 1982; Alexander & Dagdigian 1985). In this calculation, the mixing of the Hund's case b$_{\beta J}$ wavefunctions is not considered for simplicity. The cross sections can be represented for CCH as

$$\sigma_{NJF\to N'J'F'} = (2J+1)(2J'+1)(2F'+1) \times \sum_K \begin{Bmatrix} J & J' & K \\ F' & F & I(\mathrm{H}) \end{Bmatrix}^2 \begin{Bmatrix} N & N' & K \\ J' & J & S \end{Bmatrix}^2 P^K_{NN'},$$

whereas they are given for the ^{13}C species of CCH as

$$\sigma_{NJF_1F\to N'J'F_1'F'} = (2J+1)(2J'+1)(2F_1+1)(2F_1'+1) \times (2F'+1) \sum_K \begin{Bmatrix} F_1 & F_1' & K \\ F' & F & I(\mathrm{H}) \end{Bmatrix}^2 \times \begin{Bmatrix} J & J' & K \\ F_1' & F_1 & I(^{13}\mathrm{C}) \end{Bmatrix}^2 \begin{Bmatrix} N & N' & K \\ J' & J & S \end{Bmatrix}^2 P^K_{NN'}.$$

The latter equation is derived by a standard procedure for deriving reduced matrix elements under a coupled base (Edmonds 1957). In these equations,

$$P^K_{NN'} = (2N+1)(2N'+1)(2K+1) \begin{pmatrix} N' & K & N \\ 0 & 0 & 0 \end{pmatrix}^2 \sigma_{K\to 0},$$

where $\sigma_{K\to 0}$ represents the downward collisional cross section from the $N = K$ state to the ground state without consideration of the fine and hyperfine interactions. Since the collisional cross sections between CCH and H_2 are not reported, those between HCN and He (Green & Thaddeus 1974) are employed after the correction of the difference in reduced mass.

Appendix C: Simplified chemical model

A simplified chemical model shown in Fig. C.1 is considered to investigate an effect of the exchange reaction (3). According to Fig. C.1, the following rate equations are derived for C^{13}CH and ^{13}CCH:

$$\frac{\mathrm{d}[\mathrm{C}^{13}\mathrm{CH}]}{\mathrm{d}t} = k_r[\mathrm{HC}^{13}\mathrm{CH}^+][\mathrm{e}] - k[\mathrm{C}^{13}\mathrm{CH}][\mathrm{HA}^+] - k_d[\mathrm{C}^{13}\mathrm{CH}][\mathrm{O}] + k_{ex}^{(f)}[^{13}\mathrm{CCH}][\mathrm{H}] - k_{ex}^{(b)}[\mathrm{C}^{13}\mathrm{CH}][\mathrm{H}],$$

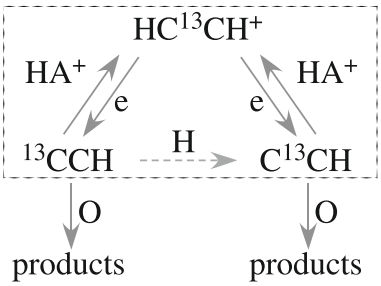

Fig. C.1. Exchange reactions between ^{13}CCH and C^{13}CH. HA$^+$ can be any ions including H_3^+ and HCO$^+$, where the proton affinity of A is lower than that of CCH.

and

$$\frac{d[^{13}CCH]}{dt} = k_r[HC^{13}CH^+][e] - k[^{13}CCH][HA^+] - k_d[^{13}CCH][O] - k_{ex}^{(f)}[^{13}CCH][H] + k_{ex}^{(b)}[C^{13}CH][H],$$

where we consider the destruction of CCH by the reaction with the oxygen atom. $[X]$ denotes the fractional abundance of X relative to H_2. Here, k_r, k, and k_d represent the rate coefficients of the electron dissociative recombination reaction of $HC^{13}CH^+$, the proton transfer reaction from HA$^+$, and the reaction with the oxygen atom. HA$^+$ can be any ions including H_3^+ and HCO$^+$, where the proton affinity of A is lower than that of CCH (6.98 eV). Furthermore, $k_{ex}^{(f)}$ is the rate coefficient of the exchange reaction (3), whereas $k_{ex}^{(b)}$ is that of the backward reaction of (3). Namely,

$$k_{ex}^{(b)} = k_{ex}^{(f)} \exp\left(-\frac{\Delta G}{kT}\right),$$

where ΔG and T represent the free energy difference of the two ^{13}C species and the temperature, respectively.

From these relations, the abundance ratio can be expressed under the steady-state approximation as

$$\frac{[C^{13}CH]}{[^{13}CCH]} = \frac{2k_{ex}^{(f)}[H] + k_d[O] + k[HA^+]}{2k_{ex}^{(b)}[H] + k_d[O] + k[HA^+]}.$$

In this equation, k_d is 1.7×10^{-11} cm^3 s^{-1} according to the UMIST database, and the fractional abundance of the oxygen atom is taken from Table 6 of Leung et al. (1984). On the other hand, k is assumed to be a Langevin rate (1×10^{-9} cm^3 s^{-1}), and [HA$^+$] is less than 10^{-8} (Leung et al. 1984). Therefore, the reaction with the oxygen atom dominates the reaction with HA$^+$, and the above equation can be simplified as

$$\frac{[C^{13}CH]}{[^{13}CCH]} = \frac{2k_{ex}^{(f)}[H] + k_d[O]}{2k_{ex}^{(b)}[H] + k_d[O]}.$$

Since $k_{ex}^{(f)}$ is uncertain, we simply assume it to be the same as k_d (1.7×10^{-11} cm^3 s^{-1}). We calculate the ratio for the two cases. One uses the atomic oxygen fractional abundance for the "early time" of the chemical model (2×10^{-4}) (Leung et al. 1984), which is appropriate for TMC-1. The other uses the atomic oxygen fractional abundance for the steady-state of the chemical model (4×10^{-5}), which is appropriate for L1527. The fractional abundance of the atomic hydrogen is also taken from the model.

Our model for TMC-1 predicts the [C^{13}CH]/[^{13}CCH] ratio to be 1.50, 1.23, and 1.08 for 10^4, 3×10^4, and 10^5 cm^{-3}, respectively. Here the temperature of 10 K is assumed and the [H] and [O] abundances of the early time are employed (Leung et al. 1984). For the density of 3×10^4 cm^{-3}, [H] is evaluated from the value for 10^4 cm^{-3} by assuming that [H] is inversely proportional to the H_2 density, whereas [O] is assumed to be the same as that for 10^4 cm^{-3}. Since the observed ratio is 1.6 ± 0.4, the model explains the ratio if the density is lower than 3×10^4 cm^{-3}. However, our model for L1527 predicts the [C^{13}CH]/[^{13}CCH] ratio to be 1.16 and 1.02 for 10^5 and 10^6 cm^{-3}, respectively. In this case, the [H] and [O] abundances at the steady state are used. These ratios are much lower than the observed ratio (1.6 ± 0.1). The low ratio calculated for L1527 originates from the low abundance of H due to the high H_2 number density, From these results, it is likely that the exchange reaction (3) would not be a main process responsible for the abundance difference between ^{13}CCH and C^{13}CH, even if the exchange reaction of (3) has no activation barrier. But there remains a small chance that it may partly contribute in TMC-1. We note that if the [O] abundance is much lower than the above estimates because of the [C]/[O] ratio close to 1, the contribution of the exchange reaction would be increased.

References

Aikawa, Y., Ohashi, N., & Herbst, E. 2003, ApJ, 593, 906
Alexander, M. H. 1982, J. Chem. Phys., 76, 3637
Alexander, M. H., & Dagdigian, P. J. 1985, J. Chem. Phys., 83, 2191
Benson, P. J., Caselli, P., & Myers P. C. 1998, ApJ, 506, 743
Caselli, P., Walmsley, C. M., Zucconi, A., et al. 2002, ApJ, 565, 344
Crofton, M. W., Jagod, M.-F., Rehfuss, B. D., & Oka, T. 1989, J. Chem. Phys., 91, 5139
Edmonds, A. R. 1957, Angular Momentum in Quantum Mechanics, Princeton, New Jergey, 109
Goldreich, P., & Kwan, J. 1974, ApJ, 189, 441
Green, S., & Thaddeus, P. 1974, ApJ, 191, 653
Hirahara, Y., Suzuki, H., Yamamoto, S., et al. 1992, ApJ, 394, 539
Hirota, T., Yamamoto, S., Mikami, H., & Ohishi, M. 1998, ApJ, 503, 717
Hirota, T., Ikeda, M., & Yamamoto, S. 2001, ApJ, 547, 814
Langer, W. D., & Graedel, T. E. 1989, ApJS, 69, 241
Langer, W. D., Graedel, T. E., Frerking, M. A., & Armentrout, P. B. 1984, ApJ, 277, 581
Langston, G., & Turner, B. 2007, ApJ, 658, 455
Leung, C. M., Herbst, E., & Huebner, W. F. 1984, ApJS, 56, 231
Lucas, R., & Liszt, H. 1998, A&A, 337, 246
McCarthy M. C., Gottlieb C. A., & Thaddeus P. 1995, JMS, 173, 303
Millar, T. J., Bennett, A., & Herbst, E. 1989, ApJ, 340, 906
Müller, H. S. P., Klaus, T., & Winnewisser, G. 2000, A&A, 357, L65
Müller, H. S. P., Schlöder, F., Stutzki, J., & Winnewisser, G. 2005, J. Mol. Struct., 742, 215
Ohashi, N., Lee, S. W., Wilner, D. J., & Hayashi, M. 1999, ApJ, 518, L41
Petrie, S. 1996, MNRAS, 281, 666
Rodgers, S. D., & Millar, T. J. 1996, MNRAS, 280, 1046
Sakai, N., Ikeda, M., Morita, M., et al. 2007a, ApJ, 663, 1174
Sakai, N., Sakai, T., Osamura, Y. & Yamamoto, S. 2007b, ApJ, 667, L65
Sakai, N., Sakai, T., Hitora, T., & Yamamoto, S. 2008, ApJ, 672, 371
Saleck, A. H., Simon, R., Winnewisser, G., & Wouterloot, J. G. A. 1994, Can. J. Phys., 72, 747
Schilke, P., Warmsley, C. M., Pineau des Forêts, G., et al. 1992, A&A, 256, 595
Sonnentrucker, P., Welty, D. E., Thorburn, J. A., & York, D. G. 2007, ApJ, 168, 58
Suzuki, H., Yamamoto, S., Ohishi, M., et al. 1992, ApJ, 392, 551
Takano, S., Suzuki, H., Ohishi, M., et al. 1990, ApJ, 361, L15
Takano, S., Masuda, A., Hirahara, Y., et al. 1998, A&A, 329, 1156
Tarroni, R., & Carter, S. 2003, J. Chem. Phys., 119, 12878
Turner, B. E. 2001, ApJ, 136, 579
Turner, B. E., Herbst, E., & Terzieva, R. 2000, ApJS, 126, 427
Watson, W.D. 1974, ApJ, 188, 35
Woods, P. M., & Willacy, K. 2009, ApJ, 693, 1360
Yamada, M., Osamura, Y., & Kaiser, R.I. 2002, A&A, 395, 1031